Biogeotechnics 4 (2026) 100183

Contents lists available at ScienceDirect

Biogeotechnics

journal homepage: www.keaipublishing.com/en/journals/biogeotechnics/

Research Article

A novel methodology for modeling the effects of geometrical uncertainties in tree root-soil geometry on tree uprooting

Mahtab Shiravi[a,b,*], Ivan Depina[a], Marco Uzielli[b], Gianni Bartoli[b]

[a] Department of Civil and Environmental Engineering, Norwegian University of Science and Technology, Norway
[b] Department of Civil and Environmental Engineering, University of Florence, Italy

ARTICLE INFO

Keywords:
Tree roots
Root-soil interaction
Uprooting
Space colonization algorithm
Embedded beam

ABSTRACT

Tree root-soil interaction is important for problems such as uprooting of trees subjected to wind loads or the stability of vegetated slopes. This paper examines the stability of laterally loaded trees (e.g., subjected to wind) and introduces a novel methodology for characterizing the uprooting capacity of tree root-soil systems. The novelty of the methodology originates from the coupling between the Space Colonization Algorithm (SCA) for the geometry characterization of the root system with an efficient Finite Element Method (FEM) model. Each tree is unique, and finding a generalized model would need to account for multiple scenarios involving different a priori uncertain tree root geometries and soil types. The proposed methodology allows for the assessment of uncertain root geometries and their effects on the mechanical response of the root-soil system, thanks to the stochastic nature of the SCA. It introduces a competitive growth algorithm that models root branch expansion in the soil as a dynamic and stochastic process. The study captures the mechanical response of a tree root system with a 3D FEM model by using an elastoplastic mechanical model for the soil, while the roots are modeled with elastoplastic embedded beams. The proposed model enables the identification of the locations of root breakage and soil failure paths in multiple scenarios. Model outputs allow quantitative investigation into the relationship between root system geometry and the root-soil system uprooting capacity and base stiffness.

1. Introduction

Trees are important for urban environments, affecting aesthetics, living quality, biodiversity, and local climate. Careful tree management is required to maintain the positive effects of trees on urban environments and reduce the risks they may impose on life, health, and property. One of the potential risks is wind throwing or uprooting of trees subjected to strong wind loads. The uprooting collapse occurs through the mechanical interaction between soil and roots, with the loading on the tree exceeding the combined bearing or anchorage capacity of the tree root-soil system (Yang et al., 2018).

Pioneering studies on tree pull tests conducted by Coutts, (1983, 1986) and Blackwell et al. (1990) identified various elements influencing tree anchorage, including the resistance of windward roots, the mass of the soil-root plate, leeward hinge resistance to bending, soil resistance in terms of shear strength, and the weight of the tree's stem and crown.

Understanding the anchorage capabilities of tree root-soil systems is crucial for assessing tree mechanical stability. Advancements in empirical and theoretical insights into root-soil interactions have been achieved through a combination of tree-pulling experiments and numerical simulations (Achim & Nicoll, 2009; Coutts, 1983; Danjon et al., 2005; Dupuy et al., 2005a; Fourcaud et al., 2008; Stokes, 1999; Yang et al., 2018).

Empirical regression models have been developed to establish the relationship between critical bending moment and key tree parameters, such as Diameter at Breast Height (DBH) and stem weight (Achim & Nicoll, 2009; Mansour et al., 2024; Nicoll et al., 2005). These models offer a straightforward approach for estimating the resisting moment without the complexities of numerical modeling. However, numerical modeling is suitable for studying the soil-root interaction mechanism during uprooting.

FEM models can range from simplified representations, such as modeling the root system as a plate resting on the soil surface with equivalent springs to capture the stiffness of the root-soil system (Achim & Nicoll, 2009; Blackwell et al., 1990; Kim et al., 2020), to more advanced models that incorporate detailed root distribution within the soil. These models can further refine our understanding of how root

* Corresponding author.
E-mail addresses: Mahtab.shiravi@unifi.it, Mahtab.shiravi@ntnu.no (M. Shiravi).

https://doi.org/10.1016/j.bgtech.2025.100183
Received 13 December 2024; Received in revised form 24 April 2025; Accepted 1 May 2025
Available online 16 March 2026

plate slip surfaces form and how root-soil interactions influence the position of the rotation axis.

More complicated models were developed by Dupuy et al. (2007) and Yang et al. (2014), who proposed 3D FEM models using beam elements that integrate realistic root system architectures obtained from destructive field tests. These models were designed to study the mechanisms of tree anchorage during uprooting and to evaluate the role of different root elements in maintaining tree stability. FEM models may have limitations in capturing large deformations (Huang et al., 2024). However, they are well-suited for modeling root-soil interactions up to the failure threshold within small strain ranges in the soil.

FEM models that simplify the geometry of root systems and their interaction with soils into a plate-soil model (e.g., Kim et al., 2020; Rahardjo et al., 2014) typically attempt to back-calculate the model properties by fitting the maximum bending moment from pull tests. Although often successful in fitting the measured bending moments, the simplified models may not completely capture the failure mechanism of the root-soil system. Alternatively, models that pursue more explicit modeling of root architecture (Dupuy et al., 2005b; Yang et al., 2014) can better capture the effects of root shape and soil properties on the tree anchorage mechanism. While these models show promising results in capturing the behavior of the root-soil system during tree overturning, the confident replication of root architecture relies on the availability of root detection analyses, which are costly, labor-intensive, and have higher computational requirements. Moreover, root system architectures are complex and vary among species or even for trees of the same species at different locations. This is especially relevant in urban areas where obstacles such as walls, roads, buildings, or human activities affect the geometry of root systems. Geometric and mechanical attributes of tree roots are influenced by environmental and genetic determinants. This biological and environmentally induced heterogeneity complicates the model-based replication of root branching patterns and investigations into the impact of root mechanical characteristics on tree stability (e.g., Mickovski et al., 2007). Devising approaches that can replicate and analyze a vast range of root system morphologies can significantly aid in generalizing investigations into the stability of trees and their resistance to mechanical failure mechanisms such as uprooting (Dupuy et al., 2007).

While previous studies have successfully employed FEM to model root-soil interaction, existing approaches either oversimplify the root system as a plate or require complex root geometry data that are often unavailable. This study bridges this gap by introducing a flexible methodology that allows for stochastic modeling of root system morphology while capturing the mechanical behavior of the root-soil system with an advanced FEM simulation, attempting an accurate representation of root-soil interactions in the context of tree stability under wind loading. A novel methodology is introduced in this paper that couples SCA for characterizing root system geometry with a three-dimensional FEM model for efficient mechanical analysis of the root-soil interaction. The uncertainty in the spatial configuration of root-soil systems is accounted for by assuming a random distribution of root geometry. The root geometry model is generated in the Plaxis 3D software (PLAXIS 3D, 2024) based on the SCA (Runions et al., 2007) that simulates competitive growth among root branches of the root system, with the branches modeled as embedded beam elements. This approach allows for efficient modeling of soil-root systems and the quantitative investigation into the effect of wind forces on mechanical stability concerning uprooting failure. The proposed methodology is flexible and can be employed to analyze variations in the shapes of tree roots for naturally growing trees and non-standard shapes for those encountered in urban areas. However, an attempt was made to compare the model output with field test data; the lack of sufficient information to replicate the root system posed challenges in effectively validating the developed model, and further field testing and analysis are necessary to calibrate the model appropriately. The paper provides a detailed insight into the algorithm and the modeling process, along with the discussion and critical assessment of the outputs.

2. Root geometry

Modeling of tree geometry has been addressed using different approaches (Hidayat et al., 2020; Li et al., 2022; Zanotto et al., 2024). Some approaches aim to utilize recursive and/or fractional patterns in tree geometries to provide realistic models of tree geometries. The use of recursive and/or fractional formulations is supported from a biological perspective with their natural growth and development process (Wilson, 1984). Honda (1971) first introduced the concept of trees as recursive structures through visual modeling of tree architectures. The study characterized trees as branching structures with a restricted set of geometric attributes, such as branching angles and length ratios of consecutive branch segments. Subsequent research enhanced the visual accuracy of these recursive models by incorporating random and systematic changes to the parameters based on the branches' placement within the overall structure of the tree (Bloomenthal, 1985; Lintermann & Deussen, 1999; Oppenheimer, 1986; Prusinkiewicz et al., 2001). While more studies suggest recursive patterns in tree branches, van Noordwijk et al. (1994) suggested that tree root architecture could also be modeled using fractal geometry. They proposed that examining the proximal roots (those directly attached to the root collar) and measuring their vertical insertion angles and diameters would be sufficient to predict total root distribution.

Sachs and Novoplansky (1995) argued that viewing a mature tree solely as a recursive structure fails to capture the full complexity of its shape, which is significantly influenced by environmental conditions. They posed that the intricate canopy structure and the tree's developmental flexibility are primarily driven by the competitive growth dynamics among its branches. Runions et al. (2007) presented SCA as an alternative to the recursive branching method in creating tree models.

SCA was implemented in this paper to simulate root structures within a soil volume. Although SCA has been primarily used for modeling the aboveground geometry of a tree, the flexible and random nature of the algorithm allows for creating root systems. This is demonstrated in Fig. 1A, with the algorithm initially establishing a three-dimensional boundary outlining the root system's overall shape. Such a boundary is versatile enough to mimic various root growth behaviors specific to different tree species, such as heart, tap, and plate root systems. In rocky areas or urban settings, where urban infrastructure can restrict the root systems' natural expansion, the modeling of root geometry can be adapted to such conditions by incorporating the impenetrable obstacles in the initial three-dimensional boundary. One of the simplest shapes is shown in Fig. 1A, where the volume to be populated with a root system is defined as a semi-ellipsoid. The three axes of the semi-ellipsoid can be adjusted to create various root geometries. For example, the depth of the root system envelope can be determined by the maximum depth of the roots, and its horizontal radius is calculated from the maximum lateral extension of the root system. By varying these parameters, characteristic dimensions of root systems for various tree species can be recreated.

Once the boundaries are created, the encompassing volume is filled with N randomly distributed attractor points (i.e., green points in Fig. 1A) in addition to the one point at the stem base. The random points indicate available space for growth of the roots, and non-uniform distributions of attractor points can be considered to fine-tune the geometry of root systems. Another important feature of the SCA algorithms is the randomness in the resulting geometry of the root system, which is the outcome of the random distribution of the attractor points. This allows for modeling effects of geometrical uncertainty of root configurations. This is of high importance as root geometry is often highly uncertain, with limited knowledge that can be gained from non-destructive tests. Modeling root geometry as uncertain allows for expressing the lack of knowledge about root geometry in a well-defined framework and quantifying the effects of uncertainties in the root system geometry.

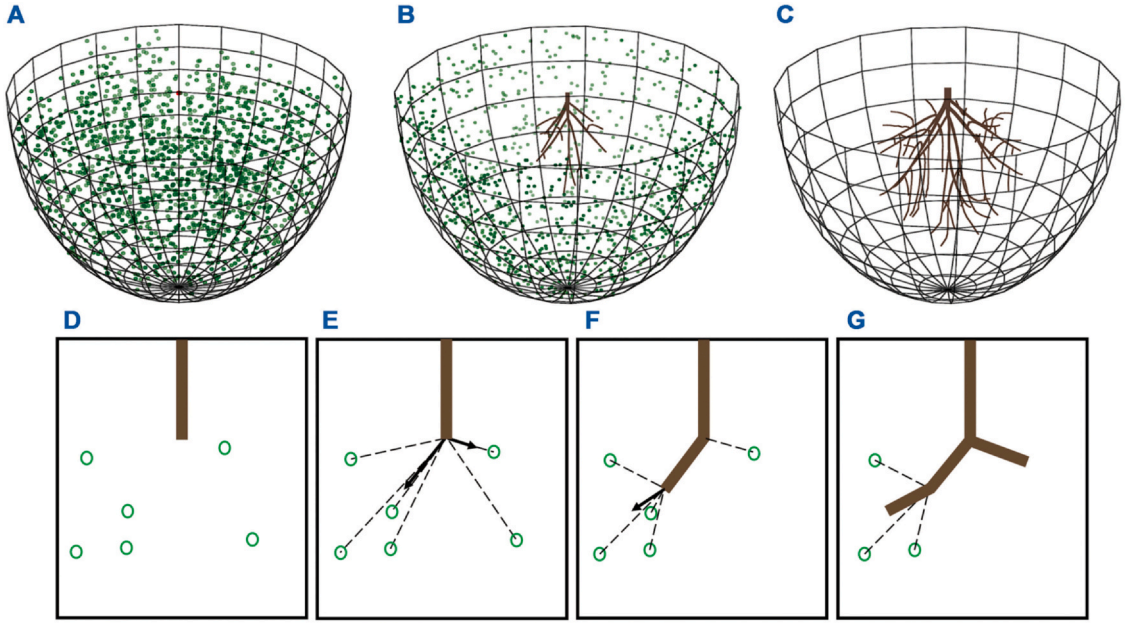

Fig. 1. (**A**) Initial boundary and distribution of attraction points; (**B–C**) Development of root skeleton; Simplified root growth algorithm: (**D**) Nodes in the radius of influence, (**E**) Resulted in normalized vectors toward the new nodes for new branches, (**F**) New nodes, and new root branches are added, (**G**) The affected attraction points are removed.

Once the attractor points are generated, the SCA iteratively generates root branches and eliminates attractor points, as shown in Fig. 1B. The mechanism for the growth of root branches and elimination of attractor points in each cycle is shown in Fig. 1D–G. Fig. 1D shows a root branch, or the stem node in case of the first iteration, and several attractor points in its vicinity. Further growth of the root system is affected by the attractor points within a predefined radius of influence, d_i, of the end node of a root branch. As shown in Fig. 1E, multiple points, collectively denoted as $S(v)$, affect the end node, v, of the root branch. If $S(v)$ is not empty, a new node, v', is formed and linked to v by a root branch, see Fig. 1F. The placement of v' is determined by calculating the mean of the normalized directions toward all influencing sources in $S(v)$, and a node is made at a pre-specified growth distance, d, from v (Runions et al., 2007). The mean direction for the branch growth is calculated as:

$$\vec{n} = \sum_{s \in S(v)} \frac{\vec{s} - \vec{v}}{\| \vec{s} - \vec{v} \|} \tag{1}$$

where $\vec{v}$ and $\vec{s}$ are vectors from the origin to the points v and s, respectively.

The normalized mean direction vector, $\hat{n}$, is obtained by normalizing $\vec{n}$:

$$\hat{n} = \frac{\vec{n}}{\|\vec{n}\|} \tag{2}$$

The end node for the root branch (v, v') is added in the direction $\hat{n}$ at a distance d:

$$\vec{v'} = \vec{v} + d\hat{n} \tag{3}$$

It is important to note that d is a parameter also affecting the development of the root geometry and it can be exploited for fine-tuning the root geometry.

The procedure concludes once all points of attraction are eliminated such that no nodes fall within the influence radii of any remaining points or after achieving a predetermined number of iterations. After adding new nodes, an evaluation is conducted to determine if any attraction points need to be eliminated because root branches have extended close to these points. Fig. 1C shows the final geometry of the root system once all of the attractor points were eliminated.

Once all the root branches are defined, the radius of the root branch is calculated by assuming that all the tips of the branches start with the same relative radius, $r_0 = 1$. This assumption can be adapted to varying radii if needed. The radii of the remaining root branches are calculated iteratively upwards from the root tips toward the tree's base. At junctions where K lower-level contributing branches of radii r_i; $i = 1, \ldots, k$ meet, the supporting higher-level branch's radius, r, is determined as follows:

$$r^2 = \sum_{i=1}^{k} r_i^{\alpha} \tag{4}$$

Where $2 \leq \alpha \leq 3$. In this study, $\alpha = 2$ is used, which corresponds to the cross-sectional area of the supporting branch being equal to the sum of the cross-sectional areas of the contributing branches. Finally, the calculated radii are scaled to match the DBH of the trunk.

Although root geometries that appear realistic can be created with the SCA, this does not necessarily guarantee that the resulting root geometry is realistic in terms of the distribution of the root mass or root cross-sectional area. Therefore, it is suggested to use additional available statistics for a given tree species to calibrate the hyperparameters of SCA (e.g., boundary geometry, distribution of attractor points, growth distance) to obtain more realistic root properties.

3. Mechanical model of the root-soil system

3.1. Introduction

Tree root geometry, modeled with SCA, is imported in a three-dimensional FEM root-soil model in Plaxis 3D geotechnical software, as shown in Fig. 2A. Wind loading was modeled using a pseudo-static force (F) applied in the positive x direction and the resultant moment (M). These actions were applied to the midpoint of the plate, along with the weight of the Above-Ground Biomass (AGB) representing the self-weight of the tree. The goal of the FEM root-soil model is to simulate the mechanical response of the root-soil system subjected to a lateral static load (e.g. mimicking the effect of the wind load). The branches of

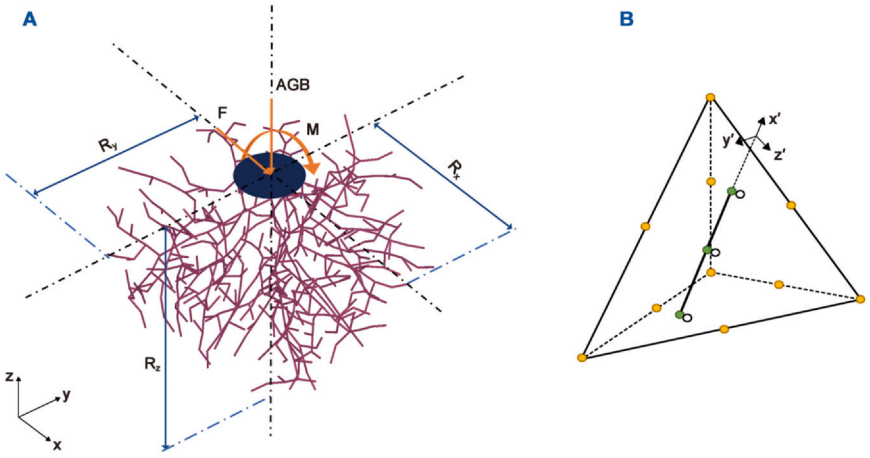

Fig. 2. (**A**) Root-soil model and applied loads; (**B**) Visual representation of embedded beam element in Plaxis 3D (PLAXIS 3D, 2024).

the root system are modeled as 'embedded beams' that allow the modeling of forces and moments in the root system. The embedded beam model allows for the possibility of accounting for elastoplastic behavior in the root system and damage due to the failure of root branches.

A rigid connection is defined between the embedded beams. Once the maximum axial force or bending moment is reached, the material exhibits plastic behavior, allowing the root to yield and deform further without rupturing. However, this approach does not account for root breakage that may occur under high mechanical stress. Capturing such failure would require a more advanced constitutive model than the Mohr-Coulomb criterion used in this study, which is limited to representing yielding behavior. Incorporating root breakage mechanisms remains an important aspect for future model development.

The failure of the root-soil system occurs within small strain ranges, and large deformations are not the primary concern, as the focus is on capturing the failure threshold.

Soil response is modeled with three-dimensional finite elements and nonlinear material behavior. Plaxis 3D includes a variety of advanced soil models that can be employed to model soil response to varying loading conditions. The interaction between the embedded beams and the soil is modeled through interface elements. The current formulations of the interface for embedded beams allow for slippage between the root and soil only in the axial direction, with the interface not accounting for potential flow-around behavior of soil in the remaining directions. In this study, slippage along the axial direction is governed by the Mohr-Coulomb frictional model, where the interface shear strength is defined by the normal stress-dependent cohesion and friction angle at the interface (Eq. 5). More details on the embedded beam model are provided in later sections. On top of the root-soil model, a plate is added with a diameter equal to the stem diameter to avoid punch-through failure mechanisms, allowing for a realistic transfer of forces and bending moments from the aboveground part of the tree to the soil and roots. Finally, model building was automated by using Python scripting in Plaxis 3D.

This modeling strategy was selected as an optimal compromise between numerical complexity and accuracy. An alternative approach could be to model roots with volume elements and interface elements that enable more accurate modeling of the interface between the roots and soil. However, such a modeling approach is met with challenges related, among others, to handling geometry intersections, requirements for very fine mesh on the outermost branches, and substantial computational demands. The modeling strategy proposed in this study successfully overcomes most of these limitations with potential limitations in the accuracy of interface modeling. These could be effectively mitigated with more advanced formulations of the embedded beam models. Beyond embedded beams, alternative approaches such as Node-to-Segment (NTS) method (Tomobe et al., 2019, 2021) have been proposed for modeling root-soil interactions. Further investigation is needed to evaluate whether NTS can provide a more effective solution for capturing complex root geometries while accurately modeling lateral resistance.

3.2. Embedded beam model of the root system

In Plaxis 3D, an embedded beam is a structural element that can be oriented in any direction within the soil volume and interacts with it through a specialized interface. The beam components are structured as three-node line elements with six degrees of freedom within a 10-noded tetrahedral element representing the soil. Unlike standard interfaces with volume piles, specialized interface elements create virtual nodes at beam nodes within the soil, linking the beam directly with all nearby soil nodes (Fig. 2B).

An embedded beam does not occupy physical space; however, an elastic zone is assumed around the beam, where the plastic behavior of the soil is prevented. The dimensions of this zone are equal to the pile's diameter as specified by the material of the beam, causing the beam to mimic a volume pile.

Embedded beams are versatile and useful for modeling various slender structures within the soil. An elastoplastic model describes the interface behavior. The interaction between the embedded beam element and soil includes skin and base resistance, and the forces exerted depend on the relative movement between the soil and the beam.

The layer-dependent setting in Plaxis 3D links local skin resistance to specific strength properties – cohesion, c, and friction angle, φ – along with the interface strength reduction factor, R_{inter}, as specified in the material data set for the relevant soil layers where the pile is installed.

The friction at the root-soil interface is influenced by multiple factors, including soil type, root surface properties, and moisture content. The selection of an appropriate R_{inter} value should be guided by experimental data, derived from pull-out experiments (e.g., Tomobe et al., 2021).

In PLAXIS, the R_{inter} defines the strength at the interface, ranging from 0 to 1, where 0 represents a perfectly smooth interface with no resistance, and 1 indicates a fully bonded interface, matching the strength of the surrounding soil.

In the analysis performed in this study, R_{inter}, is considered to be 1, assuming that the root-soil interface provides the same resistance as the surrounding soil. This parameter can be adjusted to reflect variations in interface strength, allowing for a more accurate representation of the interaction between roots and soil.

$$\tau_i = \sigma_n' \tan\varphi_i + c_i \tag{5}$$

$$\sigma_n' = \frac{\sigma_2' + \sigma_3'}{2} \tag{6}$$

$$c_i = R_{\text{inter}} c_{\text{soil}} \tag{7}$$

$$\tan\varphi_i = R_{\text{inter}} \tan\varphi_{\text{soil}} \tag{8}$$

In this context, τ_i is the local shear stress resistance of the interface, σ_n' is the normal stress, φ_i and c_i are the friction angle and cohesion of the interface, respectively. Similarly, φ_{soil} and c_{soil} are the friction angle and cohesion of the correspondent soil layer.

The skin resistance, T_i, as a force per unit of depth, is defined as Eq. (9), where R_{eq} is the embedded beam's equivalent radius.

$$T_i = 2\pi R_{\text{eq}} \tau_i \tag{9}$$

For the interface, to remain elastic, the shear force at a particular point should be less than the maximum local skin resistance, $T_{\max}$, defined in Plaxis 3D.

The base resistance, $F_{\max}$, represents the maximum force at the base of an embedded beam, defining its end-bearing capacity. It is important to note that the base can withstand compressive forces only, not tensile forces.

In addition to skin and base resistance, an embedded beam in Plaxis is characterized by its elastic modulus, E, yield stress, σ_y, and diameter.

Due to the absence of limits on the lateral shear component of the embedded beam, the interface is expected to maintain elastic properties when subjected to any lateral force. This might create an overprediction of the maximum overturning moment at the tree base. Apart from unlimited lateral resistance in the beam itself, the embedded beam can have elastoplastic behavior in bending and pulling (PLAXIS 3D, 2024).

3.3. Soil modeling

The soil is modeled as a homogeneous and isotropic porous medium with elastic, perfectly plastic behavior following the principles of the Mohr-Coulomb failure criterion. The shear strength of soil is defined as:

$$\tau_{\max} = \sigma_n \tan\varphi + c \tag{10}$$

where $\tau_{\max}$ is soil shear strength, σ_n the normal stress, φ the soil's internal friction angle, and c denotes effective soil cohesion.

3.4. Load modeling

A rigid, isotropic, and elastic plate with a diameter equal to DBH, Poisson ratio of 0.3, and depth of 0.1 m was positioned on the soil surface at the base of the trunk.

The AGB was estimated based on the model by Kebede and Soromessa (2018) with the following relationship, where H is the total height of the tree:

$$AGB = 0.623(DBH)^{1.352}(H)^{0.703} \tag{11}$$

AGB was applied to the model alongside the lateral load and its resultant moment, illustrated in Fig. 2A. In this equation, H is measured in meters, DBH in centimeters, and AGB in kilograms.

3.5. Comparative analysis of embedded beam and volume pile models of roots

Since embedded beams are used in this study to model the roots under lateral loads, this approach may overestimate the lateral capacity of the root. To address this potential issue, volume piles are compared with embedded beams. Two distinct simulations were conducted to evaluate the potential overestimation of the lateral capacity by the embedded beam method compared to volume pile models. The first simulation is a singular vertical root/pile, while the second simulation employs a more complex arrangement involving a main vertical root with three root branches (Fig. 3). By comparing these models, the impact of root structure complexity on the predicted failure load was examined. Additionally, both simulation series included variations in the ratio of diameter, DBH, to the length, L, of each root, specifically 0.12, 0.16, and 0.2, allowing for an assessment of how these ratios affect the outcomes. Further simulations incorporating varied root configurations are necessary for a comprehensive understanding of the impact of geometry; however, creating intricate root shapes with volume piles demands the generation of a fine mesh, which is challenging due to the potential for overlapping small volumes. This highlights the advantage of using embedded beams. In these models, roots were modeled as elastic material with a Modulus of elasticity $E_R = 40$ GPa and axial skin resistance $T_{\text{skin}} = 1000$ kN.

The analyses reveal that for the single pile, the embedded beam model overpredicts the ultimate capacity by 9% for $DBH/L = 0.12$, 12% for $DBH/L = 0.16$, and 13% for $DBH/L = 0.2$. In contrast, the four-pile model shows less overprediction, with values less than 1% for $DBH/L = 0.12$, 6% for $DBH/L = 0.16$, and 10% for $DBH/L = 0.2$. The behavior of the embedded beam with a smaller DBH/L ratio is closer to that of a volume pile without an interface, likely due to less flow-around effects and base contribution (Fig. 3). This similarity becomes more pronounced in the four-pile models. This indicates that for tree roots acting as slender piles, the overprediction of the ultimate capacity tends to be lower, and the embedded beam element used in simulations can closely replicate the behavior of volume piles.

Despite this level of overprediction, the embedded beam approach remains preferable due to its modeling simplicity, particularly as it avoids the inherent challenges associated with mesh generation in volume pile modeling. The comparative analysis underpins the potential of the embedded beam model, suggesting that future enhancements could refine its predictive accuracy, thereby rendering it even more effective for practical applications.

4. Case study

While the root geometries generated with SCA look realistic, it is advisable to use additional statistics available for specific tree species to adjust the root geometry and properties to achieve a more accurate root system. Future studies should explore additional statistics, such as the relationship between root diameter and length (Wu et al., 2016) or Root Length Density (RLD), which quantifies root length per unit soil volume and aids in assessing root distribution and growth patterns (Allan Jones et al., 1991). Such detailed datasets are currently limited, but establishing these statistics across different tree species would provide valuable information for refining and calibrating the proposed algorithm.

One valuable piece of information from field tests in previous works is the distribution of root cross-sectional area in depth for different species (e.g., Bischetti et al., 2009; Preti & Giadrossich, 2009). The SCA presented in this study was used to simulate a sample root system, where the Root Area Ratio (RAR), defined as the ratio of root area to the cross-sectional area of the soil affected by the roots, was calculated following the methodology of Preti et al. (2010). RAR has been shown to exhibit an exponential decrease with depth, a trend also documented by Giachi et al. (2024) in their empirical observations. The soil and the sample root model properties generated with SCA are shown in Table 1. RAR is determined using Eq. (12), where $RAR(z)$ represents the Root Area Ratio at depth z, $Ar(z)$ is the total cross-sectional area of roots at depth z, and A_{rs} denotes the rooted soil cross-sectional area (Preti et al., 2010).

$$RAR(z) = \frac{Ar(z)}{A_{\text{rs}}} = \sum_{i=1}^{m} \frac{Ar(z)_i}{A_{\text{rs}}} \tag{12}$$

The findings confirmed that the RAR values derived from the SCA simulation displayed an exponential decline with depth, aligning with natural observations (Fig. 4A). While this indicates that the algorithm can reproduce realistic root distribution trends, the study does not establish a root system directly based on RAR due to the lack of available

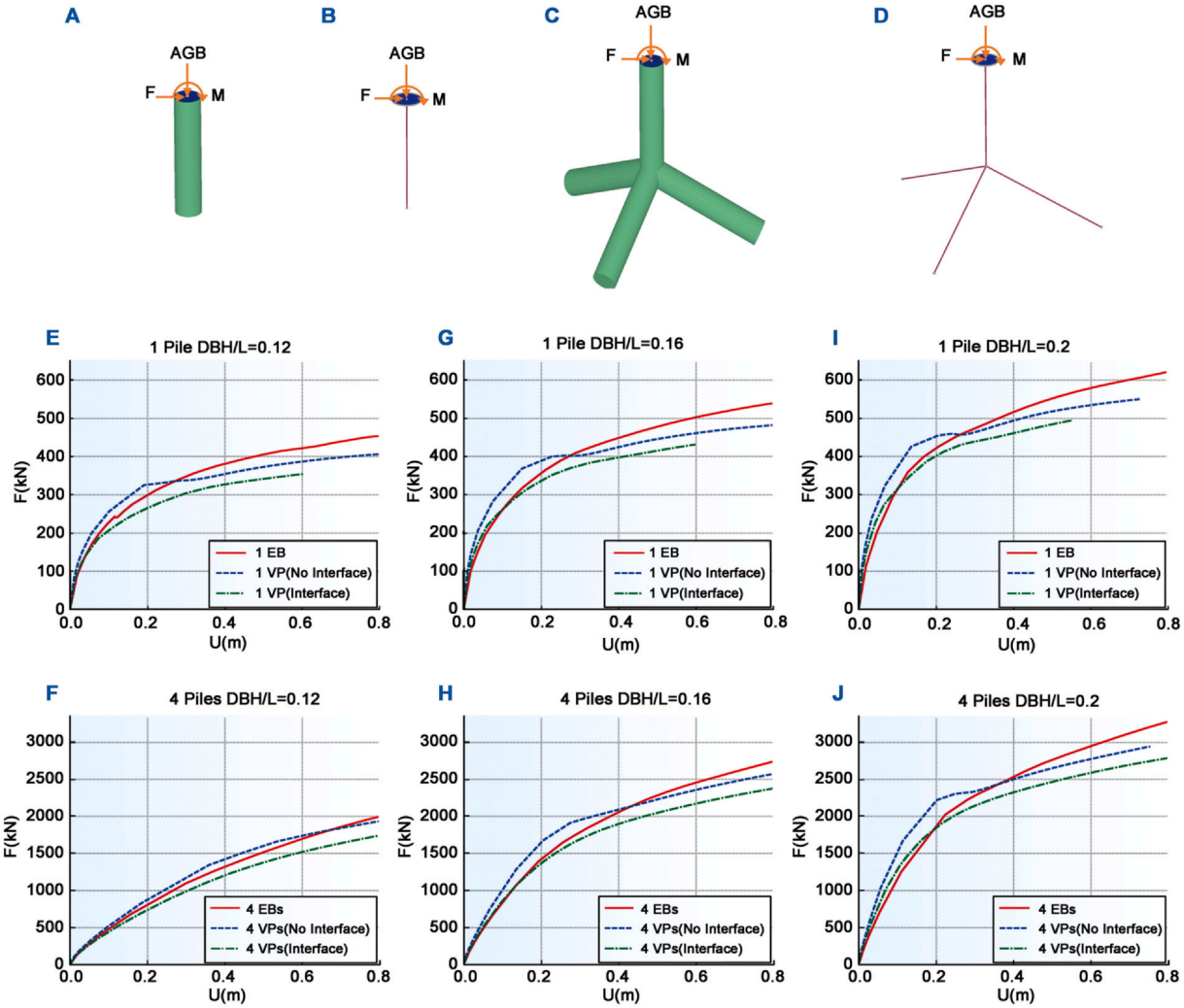

Fig. 3. (**A**) Singular vertical volume pile; (**B**) Singular vertical embedded beam; (**C**) Volume piles arrangement with a main vertical one and three branches; (**D**) Embedded beam arrangement with a main vertical one and three branches and comparison of bearing capacity of the embedded beam (EB), volume pile (VP) with the interface, and without the interface in two configurations of piles: (**E**) Single-pile model (DBH/L = 0.12), (**F**) Four-pile model (DBH/L = 0.12), (**G**) Single-pile model (DBH/L = 0.16), (**H**) Four-pile model (DBH/L = 0.16), (**I**) Single-pile model (DBH/L = 0.2), (**J**) Four-pile model (DBH/L = 0.2).

data on trees with well-documented depth-dependent RAR profiles. Although adjustments to parameters such as the number of points, root segment lengths, and root diameter scaling within the algorithm can be made to match RAR trends observed in the literature, a direct validation against measured tree root systems was not feasible.

Experimental tests, like pull-out tests, are designed to study the failure mechanisms in root-soil systems. Some studies, such as those by Dupuy et al. (2007), have attempted to model this with accurate geometries obtained from field tests. Consequently, the failure mechanism observed in the sample tree root model generated by SCA was analyzed, and it was observed that the model-predicted displacements aligned with failure mechanisms observed in pull-out tests (Dupuy et al., 2007; Rahardjo et al., 2014). Examining soil-root interactions during the tree overturning process indicates that roots on the windward side experience tensile forces as they are drawn away from the prevailing wind direction. These roots withstand significant stress as they counteract the wind force to uproot the tree. In contrast, on the leeward side, roots and soil undergo compression, stabilizing the tree against the wind direction. As the tree initiates its tilt, it rotates around a fulcrum on the leeward side, known as a “hinge” (Achim & Nicoll, 2009). The bending of leeward roots toward the soil may lead to failure, contingent on the magnitude of the force and the roots flexibility (Fig. 4B).

To illustrate the advantages of the newly developed model, the generated root geometry was compared with a simplified model employing a plate for modeling the root system. In this model (Fig. 4C), the width of the plate is equal to the maximum lateral extension of the

Table 1
Soil and root properties used in the numerical simulation with SCA.

Soil	Value	Unit	Root	Value	Unit
Modulus of elasticity (E_s)	20	MPa	Modulus of elasticity (E_R)	2	GPa
Poisson ratio (υ)	0.3	-	Axial resistance	1000	kN
Cohesion	5	kPa	Maximum depth	1	m
Friction angle	35	degree	Maximum lateral extension	2	m
			Total root volume	0.75	m^3

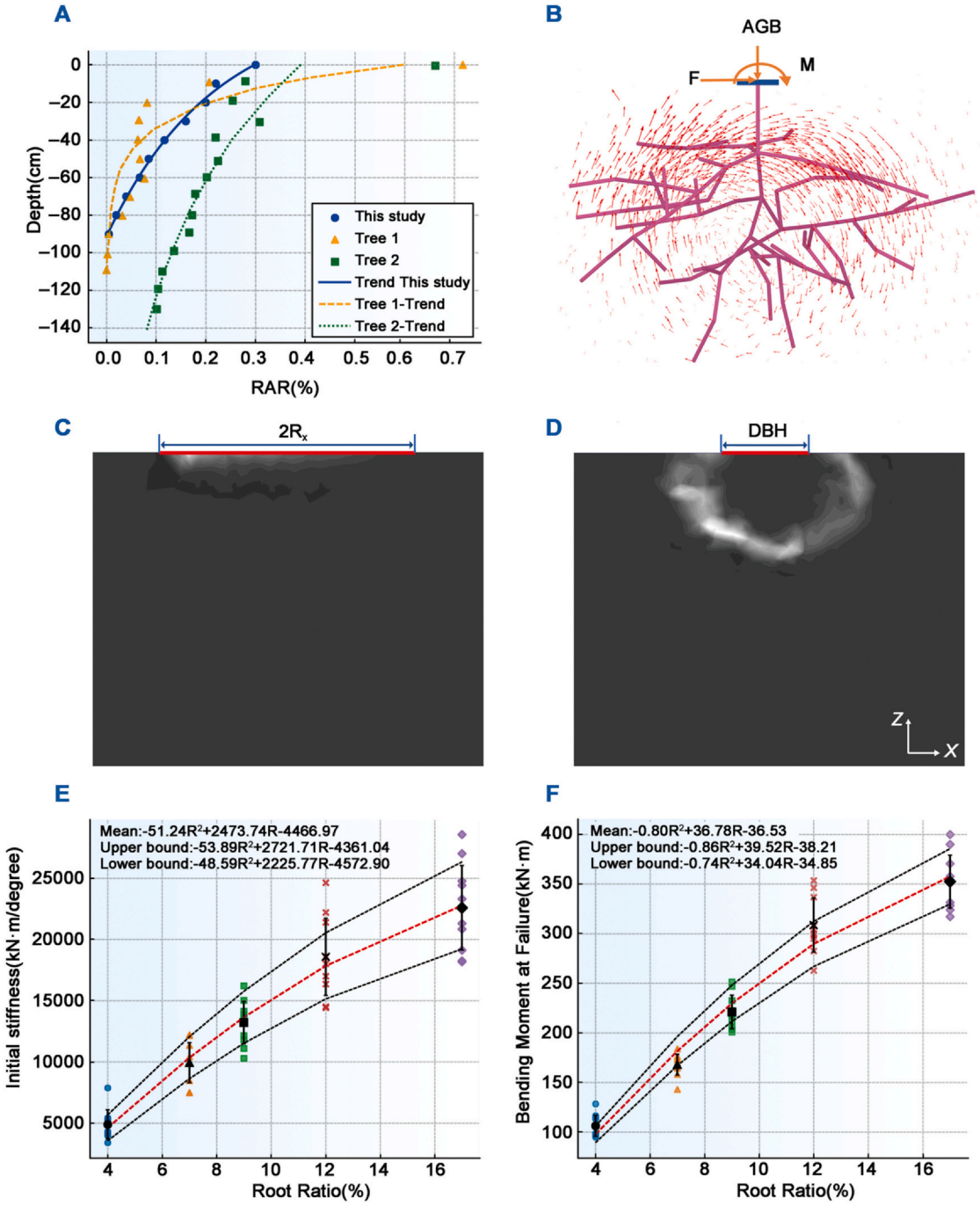

Fig. 4. (**A**) Illustration of exponential decline in RAR percentage across this study and the findings from Giachi et al. (2024); (**B**) Displacement fields at the soil in a vertical section of the Plaxis3D model; Visual comparison of deviatoric strain distribution in a vertical section when wind force is applied in the positive *x* direction: (**C**) Simplified plate model for the root system, (**D**) Proposed model in this study; (**E–F**) Effect of the stochastic simulation of root geometry on the overturning moment and base stiffness for different root ratios (R).

Table 2
Mean values and standard deviations of the failure moment and rotational stiffness across different root ratios.

	Root Ratio	0.04	0.07	0.09	0.12	0.17
Stiffness at the base (kN· m/rad)	Mean	4901	9937	13,211	18,575	22,585
	Standard deviation	1186	1625	1736	3151	3446
Bending moment(kN· m)	Mean	106	167	221	308	352
	Standard deviation	10.6	10.5	16.8	27.2	26.6

root model generated using SCA (Fig. 4D), and its modulus of elasticity corresponds to that of the roots. By using an equivalent plate, it is easier to focus on the critical interactions between the tree and the soil, avoiding the complexities associated with the detailed root architecture. This approach simplifies the analysis of how the root system tilts and how the root-soil plate resists the rotation. However, in the plate model, the failure invariably initiates at the windward plate edge, showing a shallow failure path, while the model developed in this research effectively demonstrates the strain distribution within the root-soil zone, highlighting that failure can initiate at any vulnerable point on the ground surface due to the intricate interaction between root structures and surrounding soil.

4.1. Assessing the effects of root geometry on capacity

Given the random distribution of attraction points in SCA, a series of simulations were conducted to examine how this randomness affects the load at which failure occurs and the rotational stiffness at the tree base. In these analyses, four root ratio ranges were defined, where the root ratio is the total volume of roots relative to the volume of the predefined boundary for root distribution. The simulations kept the number of attraction points, the predefined envelope size, and the soil and root properties constant, varying only the location of attraction points for each root ratio analysis. Each ratio underwent ten separate evaluations to ensure a thorough analysis of variability. The soil and root properties are those utilized in the sample root model (Table 1).

As Fig.4E–F illustrate, the failure load fluctuated between 20 and 26 percent across the different root ratios, with the most significant variability at the 0.04 root ratio. Additionally, rotational stiffness experienced a broader range of variation, spanning from 36 to 56 percent, with the highest disparity also occurring at the 0.04 root ratio. The mean and standard deviation for each variant are also shown in Table 2.

While this randomness in attraction point positions changes the configuration of root geometry and causes variation in the maximum overturning moment and base stiffness, the model effectively allows for capturing the extensive natural variability in root systems by generating root geometries randomly given the statistics of root geometries available for tree species. The current study primarily considers uncertainty in the random distribution of the attractor points in the SCA and its capacity to generate variable root systems, but it does not explicitly incorporate uncertainty in the statistical representation of root systems. Given statistical data on a specific tree species and the corresponding root properties, such as RAR distributions, a probabilistic calibration of the SCA parameters such as the placement of the boundary geometry, attraction points, growth length could be performed to generate root realizations that align with probability-based models of root systems. Future studies could explore the potential of the probabilistic calibration of the SCA parameters to capture the diversity in root system growth better and further enhance the representation of uncertainty in root architecture.

4.2. Comparative analysis of simulations and experimental test

Although the proposed model in this study demonstrates realistic behavior in the root-soil system overturning mechanism, it is often of interest to also calculate the overturning moment and the tree rotational stiffness at its base. Acknowledging that the generated root geometry is uncertain and can vary due to the random distribution of attraction points, the objective is not to validate the model precisely but to determine a range of possible stiffness values at the base and corresponding overturning moments. Additionally, SCA can create a hypothetical root geometry using available data on root mechanical properties and general geometrical information such as maximum lateral extension, depth, and total root volume. This does not exactly replicate the root geometry obtained from field tests. The main goal is to simulate realistic behavior and capture the effects of geometrical uncertainties on estimating the trees overturning capacity. If the range of possible outputs from this model is compared with field test results and demonstrates a reasonable variation around the observed values, the model could potentially replace destructive pull tests, provided some general information about the root system is known. The outputs of the approach proposed in this paper were compared with the moment-rotation curves derived from field pull-out tests and the numerical model of Yang et al. (2014). In their analysis, a 13-year-old Pinus pinaster tree with a DBH of 0.18 m was pulled out using a motorized winch. The water level was 0.6 m below the surface, with a maximum root depth of 1 m. The pulling force was exerted at 1.68 m above ground level on the tree trunk. The overturning moment was calculated from the horizontal component of this force and its point of application. Details of the soil and root characteristics applied in their numerical simulation are presented in Table 3. A model with root and soil properties similar to those described by Yang et al. (2014) was created using SCA. The generated root system maintained the same depth and lateral extension. The maximum root diameter for the root branch attached to the tree collar was scaled based on DBH. However, the total volume of the generated geometry was not available in Yang et al. (2014) work to be considered in the newly developed model. Fig. 5A compares bending moments derived from pull test data and their numerical model with the model proposed in this study.

In the research of Yang et al. (2014) the soil data were derived from field test samples and the root property data were sourced from existing literature. Due to the absence of precise mechanical properties for roots, the Modulus of Elasticity for roots is overestimated. This overestimation is discussed in Yang et al. (2014) paper, where they highlight the limitations in the available data and the challenges in accurately measuring root mechanical properties. In the overturning process simulated by SCA, initial root failure occurs at a rotational moment of 8 kN·m, characterized by bending-induced breakages, followed by a progressive reduction in the stiffness of the model until it reaches its ultimate capacity.

Table 3
Soil and root properties used in the numerical simulation (Yang et al., 2014).

Soil	Value	Unit	Root (SA2)	Root diameter	Value	Unit
Modulus of Elasticity (E_s)	19.86	MPa	Modulus of elasticity (E_R)	< 1 cm 1–6 cm > 6 cm	8.3 8.3–10.1 10.1	GPa
Poisson ratio (ν)	0.33	-	Density (ρ)	< 1 cm 1–6 cm > 6 cm	421.4 421.4–515 515	kg/m^3
Cohesion	21.402	kPa	tensile strength (t)	< 1 cm 1–6 cm > 6 cm	44.3 44.3–54.1 21.1	MPa
Friction angle	14.62	degree	compressive strength (c)	< 1 cm 1–6 cm > 6 cm	21.1 21.1–25.8 25.8	MPa

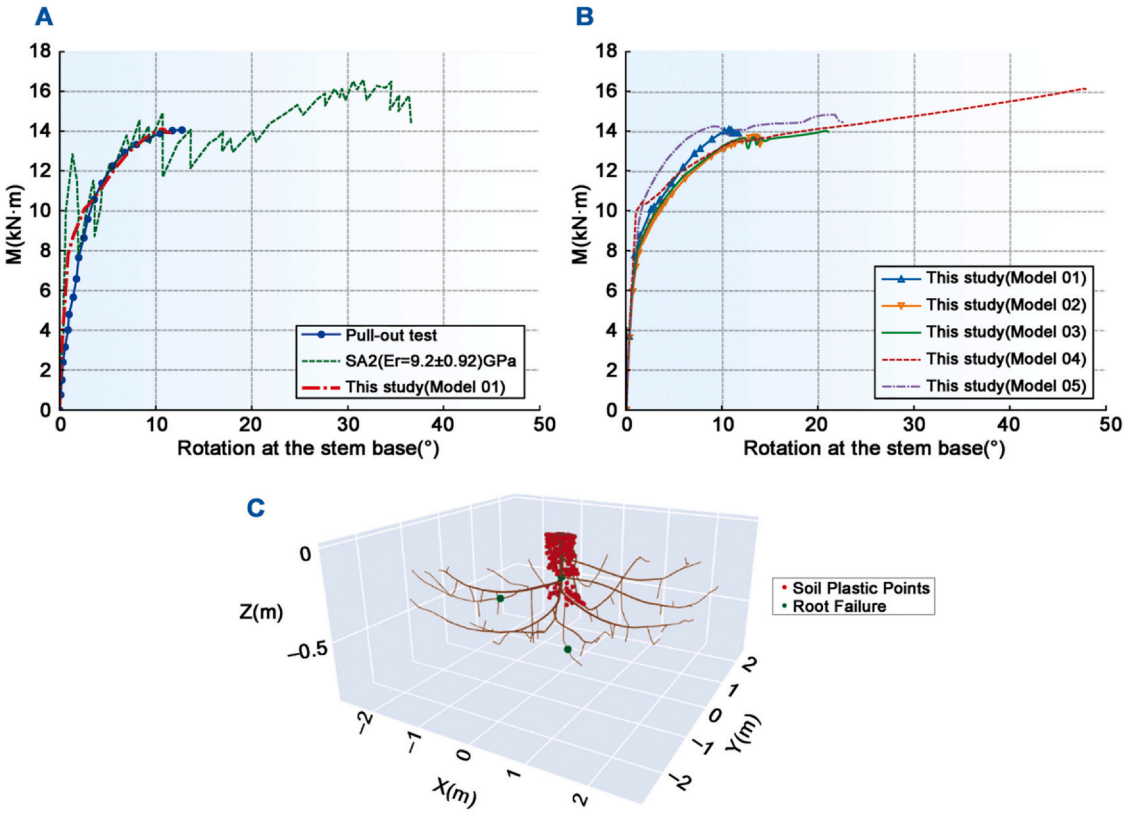

Fig. 5. (A) Comparison of bending moments derived from pull test data and numerical model of Yang et al. (2014) with the model proposed in this study; (B) The effect of randomness in the model's geometry with SCA using Yang et al. (2014) model properties; (C) Plastic points generation and root breakage in the newly developed model's initial step of root failure.

Fig. 5C illustrates the development of plastic points within the soil and the location of failure in the root at the initial failure stage of the root system when the load is applied in the positive x direction. For roots near the collar area, failure predominantly occurs due to bending forces, as these roots experience significant flexural stress under lateral loads. Roots located on the windward side of the tree, which are subjected to tensile forces, typically fail in tension. These roots may even be pulled out of the soil. This variability in root failure mechanisms is due to differences in roots mechanical properties and their position relative to the tree.

Given that SCA determines root geometry by the random distribution of attraction points within a specified boundary, the root and soil properties were kept constant, and the model was run five times to produce five different root system configurations. The analysis of variations in overturning moment and base stiffness revealed that the ultimate system capacity ranges from 13.4 to 16.12 kN·m, showing a variation of approximately 17%. Moreover, there is about a 33% variation in the initial stiffness of the tree base, which is important to consider when evaluating the accuracy and dependability of SCA in root modeling (Fig. 5B).

5. Conclusions

In this paper, a new advanced model was developed to study tree root-soil interaction under applied lateral forces using a three-dimensional FEM. The model combines SCA with embedded beam elements to generate root geometry within the soil. This approach incorporates the hypothesis of randomness in root geometry within the algorithm to capture the natural variability of root structures and simulate the competitive growth dynamics among root branches. The model demonstrates its high flexibility in generating root systems, and it could also be used when the root volume is influenced by environmental obstacles and urban infrastructures, which alter the standard natural configuration of roots. Additionally, the model can be adjusted using statistical information such as RAR from various species, enabling more precise root geometry simulations. Comparative analysis between the SCA-generated root system and a simplified plate model revealed the limitations of the plate model in simulating the failure mechanism and distribution of strain points, while the new model has promising results in simulating the expected root-soil interaction mechanism without the requirement of detailed information of root geometry and its properties. The model can estimate a potential range for initial base stiffness and maximum resisting moment using general data, such as the diameter of the first root attached to the tree base, maximum lateral extension and depth, total root volume, and the strength properties of primary roots, without necessitating destructive testing. The variation in the maximum overturning moment and base stiffness is influenced by the randomness of attraction points in the algorithm. This stochastic nature within the SCA should be accounted for when estimating each tree's failure capacity. By generating root geometries randomly, the model effectively captures the extensive natural variability in root systems, enabling a quantitative understanding of how root geometry impacts root-soil interactions.

Although the configuration of the modeled root system and its failure mechanism appear realistic, the absence of limits on the lateral shear component in embedded beams can lead to overestimating the overturning moment at the tree base. This study compares the application of embedded beams with volume piles. Due to meshing difficulties, generating a full root model with volume piles was not feasible, so two simplified configurations were analyzed. For roots/embedded beams with a smaller ratio of DBH to L, there was less difference between the ultimate capacity of the embedded beam and the volume pile. This difference decreased further in the more complex configuration of piles. Despite the potential for overprediction, the embedded

beam modeling approach is preferred over the volume pile approach due to its effectiveness in generating geometry without mesh generation issues. Further investigation is necessary to characterize and quantify the possible overprediction from the embedded beam model and the interaction mechanism between root and soil for various root sizes to determine the most appropriate modeling approach, whether it be more advanced formulations of the embedded beam models, volume piles, or a combination of both.

Despite the considerable space for further development of the proposed approach, the outputs and insights into the biomechanical aspects of tree stability highlight the significance of root architecture in enhancing tree stability, especially in environments prone to extreme weather events. The approach offers a promising tool for predicting and mitigating the risks associated with tree uprooting in urban and natural environments and for implementing effective risk management measures. Once the model is calibrated using field tests for different species and their corresponding numerical models are refined for compatibility, it can be adapted for diverse root configurations across various contexts, enhancing its applicability and utility in various scenarios.

CRediT authorship contribution statement

Mahtab Shiravi: Writing – review & editing, Writing – original draft, Visualization, Methodology, Formal analysis, Conceptualization. **Ivan Depina:** Writing – review & editing, Supervision, Methodology, Conceptualization. **Marco Uzielli:** Writing – review & editing, Methodology, Conceptualization. **Gianni Bartoli:** Writing – review & editing, Supervision, Project administration, Methodology, Conceptualization.

Declaration of Competing Interest

The authors declare that they have no known competing financial interests or personal relationships that could have appeared to influence the work reported in this paper.

Acknowledgment

The research presented in this paper was conducted as part of the RETURN project (“Multi-risk analysis for trees in urban environments”). This project is financed through the European Union's Next Generation EU initiative under PNRR Italian National funding Grant ID: B83C22004820002 (2022–2025).

References

Achim, A., & Nicoll, B. C. (2009). Modelling the anchorage of shallow-rooted trees. *Forestry, 82*(3), 273–284. https://doi.org/10.1093/forestry/cpp004

Allan Jones, C., Bland, W.L., Ritchie, J.T., & Williams, J.R. (1991). Simulation of root growth. In Modeling Plant and Soil Systems (pp. 91-123). https://doi.org/10.2134/agronmonogr31.c6.

Bischetti, G. B., Chiaradia, E. A., Epis, T., & Morlotti, E. (2009). Root cohesion of forest species in the Italian Alps. *Plant and Soil, 324*(1), 71–89. https://doi.org/10.1007/s11104-009-9941-0

Blackwell, P. G., Rennolls, K., & Coutts, M. P. (1990). A root anchorage model for shallowly rooted Sitka spruce. *Forestry: An International Journal of Forest Research, 63*(1), 73–91. https://doi.org/10.1093/forestry/63.1.73

Bloomenthal, J. (1985). Modeling the mighty maple Proceedings of the 12th annual conference on Computer graphics and interactive techniques, https://doi.org/10.1145/325334.325249.

Coutts, M. P. (1983). Root architecture and tree stability. *Plant and Soil, 71*(1), 171–188. https://doi.org/10.1007/BF02182653

Coutts, M. P. (1986). Components of tree stability in sitka spruce on peaty gley soil. *Forestry: An International Journal of Forest Research, 59*(2), 173–197. https://doi.org/10.1093/forestry/59.2.173

Danjon, F., Fourcaud, T., & Bert, D. (2005). Root architecture and wind-firmness of mature Pinus pinaster. *New Phytologist, 168*(2), 387–400. https://doi.org/10.1111/j.1469-8137.2005.01497.x

Dupuy, L., Fourcaud, T., & Stokes, A. (2005a). A numerical investigation into the influence of soil type and root architecture on tree anchorage. *Plant and Soil, 278*(1), 119–134. https://doi.org/10.1007/s11104-005-7577-2

Dupuy, L., Fourcaud, T., & Stokes, A. (2005b). A numerical investigation into the influence of soil type and root architecture on tree anchorage. *Plant and Soil, 278*(1-2), 119–134. https://doi.org/10.1007/s11104-005-7577-2

Dupuy, L. X., Fourcaud, T., Lac, P., & Stokes, A. (2007). A generic 3D finite element model of tree anchorage integrating soil mechanics and real root system architecture. *American Journal of Botany, 94*(9), 1506–1514. https://doi.org/10.3732/ajb.94.9.1506

Fourcaud, T., Ji, J. N., Zhang, Z. Q., & Stokes, A. (2008). Understanding the impact of root morphology on overturning mechanisms: A modelling approach. *Annals of Botany, 101*(8), 1267–1280. https://doi.org/10.1093/aob/mcm245

Giachi, E., Giambastiani, Y., Giannetti, F., Dani, A., & Preti, F. (2024). Root system evolution survey in a multi-approach method for SWBE monitoring: A case study in Tuscany (Italy). *Sustainability, 16*(10), https://doi.org/10.3390/su16104022

Hidayat, E.W., Giriantari, I.A.D., Sudarma, M., & Widyantara, I.M.O. (2020). Visualization of A Three-Dimensional Tree Modeling using Fractal Based on L-System. 2020 IEEE International Conference on Sustainable Engineering and Creative Computing (ICSECC).

Honda, H. (1971). Description of the form of trees by the parameters of the tree-like body: Effects of the branching angle and the branch length on the shape of the tree-like body. *Journal of Theoretical Biology, 31*(2), 331–338. https://doi.org/10.1016/0022-5193(71)90191-3

Huang, Q., Wang, Y., Leung, A. K., & Zhu, J. (2024). Large-deformation simulations of root pull-out and breakage using material point method with a multi-level grid. *Ecological Engineering, 201*, Article 107216. https://doi.org/10.1016/j.ecoleng.2024.107216

Kebede, B., & Soromessa, T. (2018). Allometric equations for aboveground biomass estimation of Olea europaea L. subsp. cuspidata in Mana Angetu Forest. *Ecosystem Health and Sustainability, 4*(1), 1–12. https://doi.org/10.1080/20964129.2018.1433951

Kim, Y., Rahardjo, H., & Tsen-Tieng, D. L. (2020). Stability analysis of laterally loaded trees based on tree-root-soil interaction. *Urban Forestry Urban Greening, 49*. https://doi.org/10.1016/j.ufug.2020.126639

Li, Z., Hao, Y., Kopp, G. A., & Wu, C.-H. (2022). Identification of multimodal dynamic characteristics of a decurrent tree with application to a model-scale wind tunnel Study. *Applied Sciences, 12*(15), https://doi.org/10.3390/app12157432

Lintermann, B., & Deussen, O. (1999). Interactive modeling of plants. *IEEE Computer Graphics and Applications, 19*(1), 56–65. https://doi.org/10.1109/38.736469

Mansour, M. A., Newson, T., & Peterson, C. J. (2024). Windthrow resistance of trees: Geotechnical engineering approach. *Trees, 38*(2), 373–391. https://doi.org/10.1007/s00468-024-02488-8

Mickovski, S. B., Bengough, A. G., Bransby, M. F., Davies, M. C. R., Hallett, P. D., & Sonnenberg, R. (2007). Material stiffness, branching pattern and soil matric potential affect the pullout resistance of model root systems. *European Journal of Soil Science, 58*(6), 1471–1481. https://doi.org/10.1111/j.1365-2389.2007.00953.x

Nicoll, B. C., Achim, A., Mochan, S., & Gardiner, B. A. (2005). Does steep terrain influence tree stability? A field investigation. *Canadian Journal of Forest Research, 35*(10), 2360–2367. https://doi.org/10.1139/x05-157

Oppenheimer, P. E. (1986). Real time design and animation of fractal plants and trees. *Proceedings of the 13th annual conference on Computer graphics and interactive techniques*. https://doi.org/10.1145/15922.15892

PLAXIS 3D. In. (2024). (Version 2024.2) Bentley Communities.

Preti, F., Dani, A., & Laio, F. (2010). Root profile assessment by means of hydrological, pedological and above-ground vegetation information for bio-engineering purposes. *Ecological Engineering, 36*(3), 305–316. https://doi.org/10.1016/j.ecoleng.2009.07.010

Preti, F., & Giadrossich, F. (2009). Root reinforcement and slope bioengineering stabilization by Spanish Broom (Spartium junceum L.). *Hydrology and Earth System Sciences, 13*(9), 1713–1726. https://doi.org/10.5194/hess-13-1713-2009

Prusinkiewicz, P., Mündermann, L., Karwowski, R., & Lane, B. (2001). The use of positional information in the modeling of plants. Proceedings of the 28th annual conference on Computer graphics and interactive techniques, https://doi.org/10.1145/383259.383291.

Rahardjo, H., Harnas, F. R., Indrawan, I. G. B., Leong, E. C., Tan, P. Y., Fong, Y. K., & Ow, L. F. (2014). Understanding the stability of Samanea saman trees through tree pulling, analytical calculations and numerical models. *Urban Forestry Urban Greening, 13*(2), 355–364. https://doi.org/10.1016/j.ufug.2013.12.002

Runions, A., Lane, B., & Prusinkiewicz, P. (2007). Modeling trees with a space colonization algorithm. In D. E. Merillou (Ed.). The Eurographics Associationhttps://doi.org/10.2312/NPH/NPH07/063-070

Sachs, T., & Novoplansky, A. (1995). Tree form: Architectural models do not suffice. *Israel Journal of Plant Sciences, 43*(3), 203–212. https://doi.org/10.1080/07929978.1995.10676605

Stokes, A. (1999). Strain distribution during anchorage failure of Pinus pinaster Ait. at different ages and tree growth response to wind-induced root movement. *Plant and Soil, 217*(1), 17–27. https://doi.org/10.1023/A:1004613126353

Tomobe, H., Fujisawa, K., & Murakami, A. (2019). Experiments and FE-analysis of 2-D root-soil contact problems based on node-to-segment approach. *Soils and Foundations, 59*(6), 1860–1874. https://doi.org/10.1016/j.sandf.2019.08.003

Tomobe, H., Fujisawa, K., & Murakami, A. (2021). A Mohr-Coulomb-Vilar model for constitutive relationship in root-soil interface under changing suction. *Soils and Foundations, 61*(3), 815–835. https://doi.org/10.1016/j.sandf.2021.03.005

van Noordwijk, M., Spek, L. Y., & de Willigen, P. (1994). Proximal root diameter as predictor of total root size for fractal branching models. *Plant and Soil, 164*(1), 107–117. https://doi.org/10.1007/BF00010116

Wilson, B.F. (1984). The Growing Tree. University of Massachusetts Press.

Wu, Q., Pagès, L., & Wu, J. (2016). Relationships between root diameter, root length and root branching along lateral roots in adult, field-grown maize. *Annals of Botany, 117*(3), 379–390. https://doi.org/10.1093/aob/mcv185

Yang, M., Defossez, P., Danjon, F., & Fourcaud, T. (2014). Tree stability under wind: Simulating uprooting with root breakage using a finite element method. *Annals of Botany, 114*(4), 695–709. https://doi.org/10.1093/aob/mcu122

Yang, M., Défossez, P., Danjon, F., & Fourcaud, T. (2018). Analyzing key factors of roots and soil contributing to tree anchorage of Pinus species. *Trees, 32*(3), 703–712. https://doi.org/10.1007/s00468-018-1665-4

Zanotto, F., Grigolato, S., Schindler, D., & Marchi, L. (2024). Identifying wind-tree dynamics with numerical simulations based on experimental modal analysis. *Forest Ecology and Management, 569*. https://doi.org/10.1016/j.foreco.2024.122188